

Multi-color solitons and frequency combs in microresonators

CURTIS R. MENYUK,^{1,*} PRADYOTH SHANDILYA,¹ LOGAN COURTRIGHT,¹ GRÉGORIE MOILLE,^{2,3} AND KARTIK SRINIVASAN^{2,3}

¹Computer Science and Electrical Engineering Department, University of Maryland Baltimore County, Baltimore, MD 21250, USA

²Joint Quantum Institute/NIST, University of Maryland, College Park, MD 20742, USA

³Microsystems and Nanotechnology Division, National Institute of Standards and Technology, Gaithersburg, MD 20899, USA

*menyuk@umbc.edu

Abstract: Multi-color solitons that are parametrically created in dual-pumped microresonators generate interleaved frequency combs that can be used to obtain combs at new frequencies and when synchronized can be used for low-noise microwave generation and potentially as an element in a chip-scale clockwork. Here, we first derive three-wave equations that describe multi-color solitons that appear in microresonators with a nearly quartic dispersion profile. These solitons are characterized by a single angular group velocity and different angular phase velocities. We then use these equations to explain the interleaved frequency combs that are observed at the output of the microresonator. Finally, we used these equations to describe the experimentally-observed soliton-OPO effect. In this effect, the pump frequency color interacts nonlinearly with a signal frequency color to create an idler frequency color in a new frequency range, somewhat analogous to an optical parametric oscillation (OPO) process, but in which the Kerr nonlinearity plays a role in matching the angular group velocity, analogous to soliton formation. These three colors then create an interleaved frequency comb in the output waveguide. We determine the conditions under which we expect this effect to occur. We anticipate that the three-wave equations and their extensions will be of use in designing new frequency comb systems and determining their stability and noise performance.

1. Introduction

It was recently discovered that it is possible to synchronously lock two comb teeth over an octave of bandwidth in a single microresonator through an all-optical, $\chi^{(3)}$ -mediated process [1]. This discovery is a significant step towards the development of a chip-scale optical clock, among other potential applications [2]. In [1], the authors use a primary pump to generate a soliton in the microresonator at around 286 THz and a reference pump at around 194 THz. The comb lines generated by the soliton are separated by around 1 THz. When the reference pump is sufficiently close to one of the soliton comb teeth, this tooth is captured by the reference pump. The back-reaction of the soliton creates a dispersive wave at nearly twice the frequency of the reference pump, which can then be locked by standard f - $2f$ self-referencing. At that point, the entire frequency comb inherits a linewidth on the order of the pump linewidths [1, 3]. The comb tooth that is pumped is locked along with all the other comb teeth.

This discovery was enabled by the earlier ground-breaking work that established the utility of a secondary pump for taming the thermal instability [4–6] that had made the generation of soliton frequency combs in microresonators a difficult, non-deterministic process. In [4–6], the secondary pump did not participate in the Kerr-mediated processes. Subsequent to that work, it was discovered that by allowing the secondary pump to participate in the Kerr-mediated processes, the secondary pump could also be used to generate an interleaved comb with a total bandwidth of 1.6 octaves in a microresonator with a large free spectral range and a carefully engineered dispersion [7]. We illustrate this configuration schematically in Fig. 1(a). It was also

observed that the secondary pump produces a secondary frequency comb, referred to here as the signal comb, with the same free spectral range (FSR) as the comb generated by the primary pump, but with a constant frequency offset. In this experiment, a third set of parametrically-induced comb lines was observed at a frequency on the opposite side of the primary pump frequency, referred to here as the idler comb. While not reported in [7], this higher-frequency idler comb was observed to have an offset from the primary comb that was just equal and opposite to the offset of the signal comb.

A qualitative explanation of this phenomenon can be given as follows: A multi-color soliton is created in the microresonator cavity that has three distinct components. A multi-color soliton is a waveform that consists of several distinct components, each of which has its own (angular) phase velocity, while they all have the same (angular) group velocity. We refer to each of these distinct components as a “color.” These multi-color solitons are somewhat analogous to solitons at multiple frequencies [8, 9] or two polarizations [10] that can propagate in optical fibers. They are also somewhat analogous to simultons that have been observed in optical parametric oscillators (OPOs) [11] and described theoretically in aluminum nitride microcavities [12]. Finally, these multi-color are similar to the multi-color solitons that are theoretically described by Luo et al. [13] and Silvestri et al. [14], although the multi-color solitons described by these authors produce spectrally distinct frequency combs, rather than the interleaved frequency combs that were experimentally observed in [7] and that we describe here.

A multi-color soliton generates a stream of pulses in the coupling waveguide that in turn generates a frequency comb when detected in a spectrometer. Because each color in the soliton has its own (angular) phase velocity, each color produces a comb with a different carrier envelope offset frequency f_{ceo} , and the combs they produce are interleaved. We schematically illustrate the multi-color soliton that produces interleaved frequency combs in Fig. 2 and the accompanying visualization. The color of the multi-color soliton that produces the idler comb must be phase-matched such that $f_{\text{ceo}+} = 2f_{\text{ceo}0} - f_{\text{ceo}-}$ in order to produce the observed frequency offset in the idler comb. In this schematic illustration, the signal color and idler color are not localized in the azimuthal angle ϕ that circulates around the cavity at the group velocity in contrast to the primary comb, which is localized. We will show that this behavior is characteristic of the multi-color solitons that generate the interleaved frequency combs.

However, obtaining a quantitative understanding is not trivial. It is not sufficient to simply solve a variant of the Lugiato-Lefever equation [15–17] that has been used with great success to understand many features of microresonator solitons and the combs that they generate. Within the microresonator, each color has a single frequency in the coordinate system that moves with the soliton’s group velocity. It is only through the detection process when a periodic stream of pulses emerges from the coupling waveguide and is experimentally detected that a frequency comb is created. To observe the interleaved comb numerically using the Lugiato-Lefever Equation (LLE), one must reproduce this stroboscopic observation process by creating a long stream of pulses and then computing the frequency transform after appropriately filtering the output [1, 7]. In Fig. 1 and the accompanying visualization, we show a schematic illustration of this process.

Here, we will show that it is possible to shortcut this numerical procedure and at the same time gain insight into the behavior of these multi-color-soliton waveforms by using three-wave equations that we will derive and that govern the behavior of the solitons that produce the interleaved comb spectrum that was described in [7]. We will show that the higher-frequency idler comb previously described is generated through a process that is somewhat analogous to the optical parametric oscillation (OPO) that occurs in continuous wave (CW) systems when a pump wave and a signal wave combine to produce an idler wave. In contrast however to the case of a CW-OPO, where both the group and phase velocities must be matched, the group velocities are automatically matched via the generation of a multi-color soliton, and it is only necessary to match the phase velocities. We will then show the precise conditions under which Eqs. 2 and 3

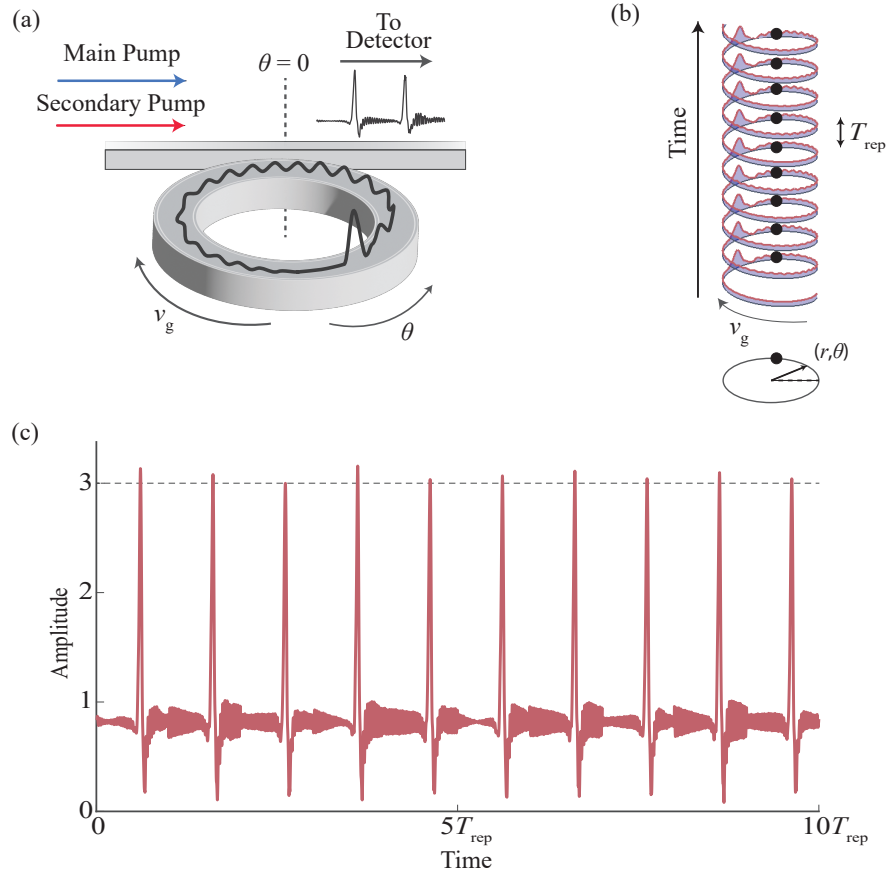


Fig. 1. Illustration of the stroboscopic process that creates a frequency comb. In (a), we show the microresonator-waveguide configuration that produces an interleaved frequency comb using both a primary and a secondary pump. As the soliton, shown propagating in the $-\theta$ -direction in (b), circulates around the microresonator, its intensity closest to the waveguide is transferred to the waveguide, which creates a periodic stream of pulses in the output waveguide, as shown in (c). Visualization 1 shows the time evolution of this process. When detected at the output of the waveguide, the stream of pulses creates an interleaved comb.

in [7] that describe the soliton-OPO effect hold.

While the multi-color solitons that we describe here are somewhat analogous to solitons in two polarizations or for that matter to solitons in any two distinct transverse modes, there is an important distinction. In the case that we are considering here, there is only a single transverse mode family, and each longitudinal mode in this family can oscillate at multiple frequencies, rather than spatially-distinct modes each oscillating at a single frequency. As a result, any computational method that simply plots the intensity of modes in the microresonator averaged over time will fail to observe the interleaved frequency combs. Rather, one must use a computational method that reproduces in some way the stroboscopic observation process outside the microresonator that separates out the distinct frequencies in each of the interleaved frequency combs.

The equations that we derive here have applications beyond the explanation of the results in [7].

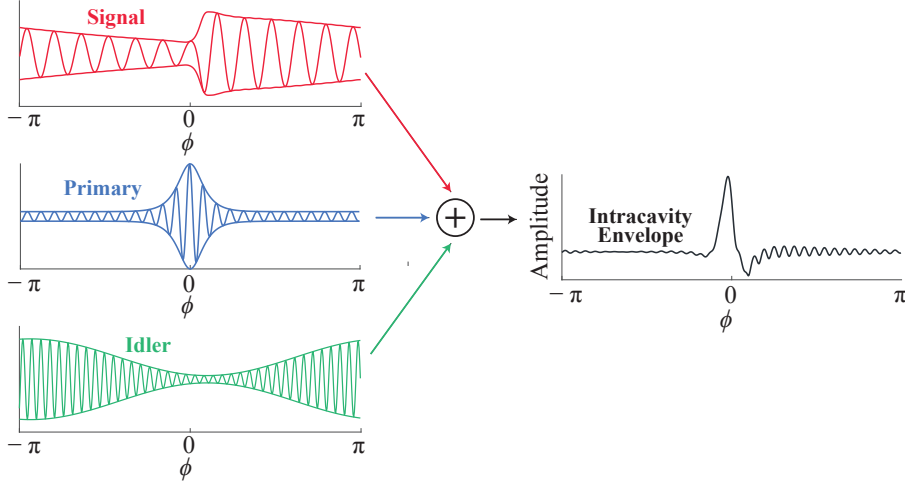


Fig. 2. A schematic illustration of a multi-color soliton. Visualization 2 shows the evolution of the waveform as a function of time. Each component has a well-defined envelope that propagates without changing, as shown on the left. On the right, we show the total field, whose envelope changes as the soliton evolves.

The integrated dispersion profile in [1] $D_{\text{int}}(\mu)$ is nearly quartic like that of the dispersion profile that produces doubly-dispersive waveguides [18]. In the case of [7], the zero-crossings are too far away from the primary pump to generate significant dispersive waves. The spectra in [7] and [18] are two examples of a family of spectra that can be produced by similar broadband microresonators. Other possibilities exist, including the configuration in [1] in which the reference pump generates a distinct color on the long wavelength side of the primary pump, while a dispersive wave is generated on the short wavelength side. This entire family of devices can be described using the three-wave equations that we derive here. Finally, these equations are the starting point for describing an OPO-soliton cascade.

2. Derivation of the Three-Wave Equations

Our starting point is an extended LLE, which in the mode number domain may be written

$$\begin{aligned} \frac{d\hat{A}(m,t)}{dt} = & iD(m)\hat{A}(m) - \frac{l}{2}\hat{A}(m,t) - i\gamma \sum_{n,p} \hat{A}(m+n-p,t)\hat{A}^*(n,t)\hat{A}(p,t) \\ & + \sqrt{\kappa_0} \delta(m-m_0)E_0 \exp(i\omega_0 t) + \sqrt{\kappa_-} \delta(m-m_-)E_- \exp(i\omega_- t) \end{aligned} \quad (1)$$

where $\hat{A}(m)$ is the field amplitude in the m -th azimuthal mode, normalized so that $|A(m)|^2$ is the energy in that mode, $D(m)$ is the linear dispersion of the m -th mode, l is the loss, whose m -dependence we neglect, γ is the Kerr coefficient, whose m -dependence we also ignore, E_0 and E_- are the primary and secondary pump amplitudes, normalized so that $|E_0|^2$ and $|E_-|^2$ are the pump powers, m_0 and m_- are the corresponding mode numbers at which they are resonant, $\sqrt{\kappa_0}$ and $\sqrt{\kappa_-}$ are the corresponding coupling coefficients, and ω_0 and ω_- are the corresponding angular pump frequencies. Here, we use $\delta(\cdot)$ to denote the Kronecker delta function or the Dirac delta function, depending on whether its argument is discrete or continuous. In Eq. 1, where m must be an integer, it denotes a Kronecker delta function. The sum in Eq. 1 is over all integer values of n and p . In general, discrete sums will denote sums over all possible values. In the

azimuthal domain (θ), Eq. 1 becomes

$$\begin{aligned} \frac{\partial \hat{a}(\theta, t)}{\partial t} = & i \sum_m D(m) \hat{A}(m) \exp(im\theta) - \frac{l}{2} \hat{a}(\theta, t) - i\gamma |\hat{a}(\theta, t)|^2 \hat{a}(\theta, t) \\ & + \sqrt{\kappa_0} E_0 \exp(i\omega_0 t + im_0\theta) + \sqrt{\kappa_-} E_- \exp(i\omega_- t + im_- \theta), \end{aligned} \quad (2)$$

where $\hat{a}(\theta, t)$ and $\hat{A}(m, t)$ are an azimuthal Fourier transform pair. We generally use x and X to denote the Fourier transform pairs that are related via the relations

$$X(m) = \int_{-\pi}^{\pi} x(\theta) \exp(-im\theta) \frac{d\theta}{2\pi}, \quad x(\theta) = \sum_m X(m) \exp(im\theta). \quad (3)$$

Equation (1) presumes that only one mode family plays a significant role in the dynamics.

We now let $\hat{a}(\theta, t) = \bar{a}(\theta, t) \exp(i\omega_0 t + im_0\theta)$, and we let $\mu = m - m_0$, so that $\mu_- = m_- - m_0$. Equation (2) then becomes

$$\begin{aligned} \frac{\partial \bar{a}(\theta, t)}{\partial t} = & i \sum_{\mu} [D(m_0 + \mu) - \omega_0] \bar{A}(\mu, t) \exp(i\mu\theta) - \frac{l}{2} \bar{a}(\theta, t) - i\gamma |\bar{a}(\theta, t)|^2 \bar{a}(\theta, t) \\ & + F_0 + F_1 \exp[i\Delta\omega_- t + i\mu_- \theta], \end{aligned} \quad (4)$$

where $\Delta\omega_- = \omega_- - \omega_0$, $F_0 = \sqrt{\kappa_0} E_0$, $F_- = \sqrt{\kappa_1} E_1$, and $\bar{A}(\mu, t) = \int_{-\pi}^{\pi} \bar{a}(\theta, t) \exp(i\mu\theta) (d\theta/2\pi)$. We next write $D(m_0 + \mu) = D^{(0)} + D^{(1)}\mu + D_{\text{int}}(\mu)$, where $D^{(0)}$ and $D^{(1)}$ are the zeroth and first order coefficients of the difference expansion of $D(m_0 + \mu)$. Equation 4 now becomes

$$\begin{aligned} \frac{\partial \bar{a}(\theta, t)}{\partial t} = & \left(i\alpha_0 - \frac{l}{2} \right) \bar{a}(\theta, t) + D^{(1)} \frac{\partial \bar{a}(\theta, t)}{\partial \theta} + i \sum_{\mu} D_{\text{int}}(\mu) \bar{A}(\mu) \exp(i\mu\theta) \\ & - i\gamma |\bar{a}(\theta, t)|^2 \bar{a}(\theta, t) + F_0 + F_1 \exp(i\Delta\omega t + i\mu_- \theta), \end{aligned} \quad (5)$$

where $\alpha_0 = D^{(0)} - \omega_0 = D(m_0) - \omega_0$ is the detuning of the primary mode resonance from the primary pump and $\Delta\omega = \omega_- - \omega_0$ is the radial frequency separation between the secondary and primary pumps .

We now specialize to the case where a multi-color soliton has formed so that the waveform is characterized by a single (angular) group velocity, $\omega_{\text{rep}} = 2\pi f_{\text{rep}} = 2\pi/T_{\text{rep}}$, where f_{rep} is the free spectral range (FSR) and T_{rep} is the round-trip time of the soliton. We can transform the coordinate system in order to freeze the soliton group velocity by letting $\phi = \theta + \omega_{\text{rep}}t$, and defining $a(\phi, t) = \bar{a}(\theta + \omega_{\text{rep}}t, t)$. Consistent with Fig. 1, we are assuming that the soliton is moving in the $-\theta$ direction. We then find the multi-pumped Lugiato-Lefever Equation (MLLE)

$$\begin{aligned} \frac{\partial a(\phi, t)}{\partial t} = & \left(i\alpha - \frac{l}{2} \right) a(\phi, t) + \beta \frac{\partial a(\phi, t)}{\partial \phi} + i \sum_{\mu} D_{\text{int}}(\mu) A(\mu) \exp(i\mu\phi) \\ & - i\gamma |a(\phi, t)|^2 a(\phi, t) + F_0 + F_1 \exp(i\delta\omega t + i\mu_- \phi), \end{aligned} \quad (6)$$

where $\beta = D^{(1)} - \omega_{\text{rep}}$, $A(\mu, t) = \bar{A}(\mu, t) \exp(-i\omega_{\text{rep}}t)$, and $\delta\omega = \Delta\omega - \mu_- \omega_{\text{rep}}$. The ϕ - μ Fourier transform pairs are: $X(\mu) = \int_{-\pi}^{\pi} x(\phi) \exp(-i\mu\phi) (d\phi/2\pi)$ and $x(\phi) = \sum_{\mu} X(\mu) \exp(i\mu\phi)$. The parameter β represents the offset between the angular group velocity at the principal mode and the actual group velocity of the waveform. In the case of interest to us, the parameter β is nearly zero, but it will not be exactly zero since the actual group velocity of the soliton is determined by a weighted mean of the group velocities of both pumps [1]. The result is a tilt in the experimentally-measured spectrum relative to D_{int} [7]. The parameter $\delta\omega$ equals the offset

between the difference of the two pump frequencies and the difference of the corresponding comb line frequencies. This offset is typically large compared to the detuning α_0 [7] and must be compensated in order for phase-matching to occur.

In general, Eq. 6 has no stationary solutions except in the case of Kerr-induced synchronization [1]. The quantity $\delta\omega$ can be as large as $\pm\delta\omega_{\text{rep}}/2$. In the limit of interest to us in which a multi-color soliton has formed, we can obtain a coupled set of equations that has stationary solutions by making the substitution

$$a(\phi, t) = b_-(\phi, t) \exp(i\delta\omega t + i\mu_-\phi) + b_0(\phi, t) + b_+(\phi, t) \exp(-i\delta\omega t - i\mu_-\phi), \quad (7)$$

where it is assumed that b_0 , b_- , and b_+ all vary slowly in time compared to $(\delta\omega)^{-1}$. We will refer to b_0 , b_- , and b_+ as the pump, signal, and idler colors, and we will refer to the combs that they produce in the output waveguide as the pump, signal, and idler combs. We will show that the component proportional to b_+ is generated by a four-wave-mixing process that is somewhat analogous to the creation of new frequencies that are generated by continuous wave (CW) OPOs. In the case of CW-OPOs it is necessary to match both the phase and group velocities. In the case of a soliton-OPO described here, the group velocities are automatically matched by the Kerr nonlinearity, and it is only necessary to match the phase velocities. We also note that when the dispersion is sufficiently flat over the bandwidth of the microresonator and $|\mu_-|$ is sufficiently small, it is possible to cascade the OPO to obtain multiple harmonics, as shown experimentally in [19]. This cascade is again somewhat analogous to a similar cascade that can occur in CW-OPOs. The cascade can be treated theoretically by letting $a(\phi, t) = \sum_{\sigma} b_{\sigma}(\phi, t) \exp(i\sigma\delta\omega t + i\sigma\mu_-\phi)$, where σ extends over the range where it is possible to match the phases velocities. In this paper, we restrict ourselves to the case where $\sigma = \pm 1$, which is sufficient to explain the experimental results in [7].

We now substitute Eq. 7 into Eq. 6, and we only keep phase-matched terms. We thus obtain

$$\begin{aligned} \frac{\partial b_0(\phi, t)}{\partial t} = & \left(-\frac{l}{2} + i\alpha_0\right) b_0(\phi, t) + i \sum_{\mu} [\beta\mu + D_{\text{int}}(\mu)] B_0(\mu, t) \exp(i\mu\phi) \\ & - i\gamma \left(|b_0(\phi, t)|^2 + 2|b_-(\phi, t)|^2 + 2|b_+(\phi, t)|^2 \right) b_0(\phi, t) \\ & - 2i\gamma b_-(\phi, t) b_+(\phi, t) b_0^*(\phi, t) + F_0, \end{aligned} \quad (8a)$$

$$\begin{aligned} \frac{\partial b_-(\phi, t)}{\partial t} = & \left[-\frac{l}{2} + i(\alpha_0 - \delta\omega + \beta\mu_-) \right] b_-(\phi, t) \\ & + i \sum_{\mu'} [\beta\mu' + D_{\text{int}}(\mu' + \mu_-)] B_-(\mu', t) \exp(i\mu'\phi) \\ & - i\gamma \left(2|b_0(\phi, t)|^2 + |b_-(\phi, t)|^2 + 2|b_+(\phi, t)|^2 \right) b_-(\phi, t) \\ & - i\gamma b_0^2(\phi, t) b_+^*(\phi, t) + F_-, \end{aligned} \quad (8b)$$

$$\begin{aligned} \frac{\partial b_+(\phi, t)}{\partial t} = & \left[-\frac{l}{2} + i(\alpha_0 + \delta\omega - \beta\mu_-) \right] b_+(\phi, t) \\ & + i \sum_{\mu''} [\beta\mu'' + D_{\text{int}}(\mu'' - \mu_-)] B_-(\mu'', t) \exp(i\mu''\phi) \\ & - i\gamma \left(2|b_0(\phi, t)|^2 + 2|b_-(\phi, t)|^2 + |b_+(\phi, t)|^2 \right) b_+(\phi, t) \\ & - i\gamma b_0^2(\phi, t) b_-^*(\phi, t). \end{aligned} \quad (8c)$$

where $\mu' = \mu - \mu_-$ and $\mu'' = \mu + \mu_-$. The tilt due the difference between the soliton group velocity and $D^{(1)}$ is now explicit in the terms $i\beta\mu_- b_-$ and $-i\beta\mu_- b_+$ that appear in these equations.

We observe that the b_+ component is driven by the term $b_0^2 b_-$, which is analogous to the driving term in a CW OPO; the ‘0’ mode is the pump, the ‘-’ mode is the signal, and the ‘+’ mode is the idler. We are assuming that the energy in the 0 mode is large compared to energy in the - mode; otherwise, additional modes could appear in the cascade. We previously noted that typically $|\delta\omega| \gg |\alpha|$ and is on the order of ω_{rep} . In order to compensate for this large offset so that the phase velocities match, D_{int} must be of the same order. As a result, the mode numbers at which phase-matching occurs and a resonant interaction is observed are shifted from μ_- and $\mu_+ = -\mu_-$.

3. Interleaved Frequency Combs and the Soliton-OPO

To demonstrate the validity of Eq. 8, we compare the solution of Eq. 8 to Eq. 6 using the same measured dispersion curve as in [7] and that we show in Fig. 3. We set $F_0 = 158$ mW, $F_- = 0.16$ mW, and $\mu_- = -90$. We have $\alpha = -3.3$ GHz, $\beta = 2.7$ GHz, $D_{\text{int}}(\mu_-) = 79.7$ GHz and $D_{\text{int}}(\mu_+) = -19.3$ GHz. The zero-crossings of $\alpha \mp \delta\omega + \beta\mu + D_{\text{int}}(\mu)$ occur approximately at $\mu = 78$ and $\mu = -138$. In steady state, the phase of each color rotates at its own frequency, so that $B_{0,-,+}(\mu, t) = B_{0,-,+}(\mu, t=0) \exp(iD_{0,-,+}t)$, where $D_{0,-,+}$ are the phase rotation frequencies of each of the colors. These are constant as a function of μ and are different for each color. These frequencies correspond to the difference between the angular phase velocity and the angular group velocity for each of the colors. In Fig. 3, we compare the time average of the energy $|A(\mu, t)|^2$ ($\langle |A|^2 \rangle$) to the stationary energies $|B_0(\mu, t)|^2$, $|B_-(\mu + \mu_-, t)|^2$, and $|B_+(\mu - \mu_-, t)|^2$, and the energies in each of the sub-components sums to the energy in $\langle |A|^2 \rangle$. This spectrum agrees reasonably well with the computational and experimental spectra reported in [7]. We neglect the change in the output coupling with mode number so that the output frequency comb spectra that are generated in the output waveguide are proportional to the mode number spectra of the colors inside the microresonator.

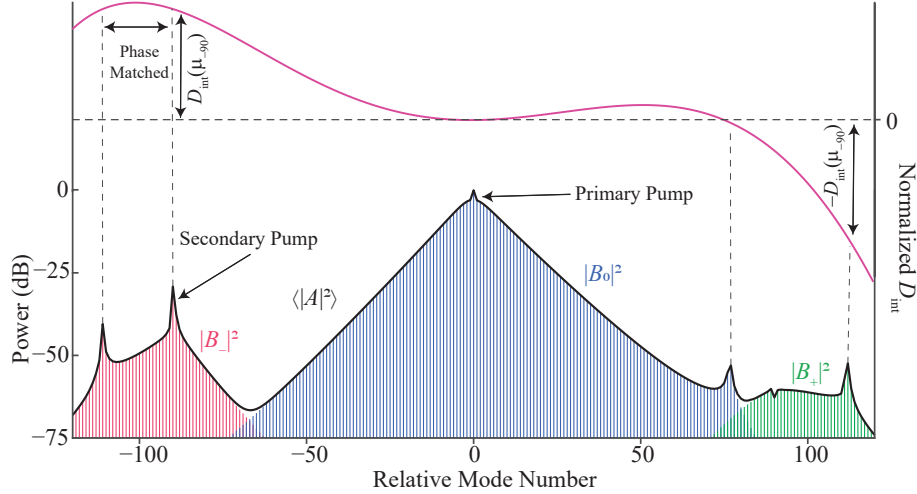


Fig. 3. Comparison of the average energy $\langle |A|^2 \rangle$ of a multi-color soliton that is calculated using Eqs. 6 and 8 normalized to the primary pump power. The energy of the three colors $|B_-|^2$, $|B_0|^2$, and $|B_+|^2$ that are computed using the three-wave equations, Eq. 8, add up to the average energy using the MLLE, Eq. 6, in the wavenumber domain.

It is the observation of a long string of pulses at the output of a coupling waveguide that produces a frequency comb from the soliton that circulates within a microresonator. In order to observe an interleaved frequency comb when simulating the experimental system [7] using Eq. 6, we can generate a long string of pulses and compute the string’s power spectral density

(PSD). The linewidth that is observed will be inversely proportional to the length of the pulse string. In Fig. 4.a, we show the PSD that is generated using Eq. 6 for the same systems as in Fig. 3. We used a string of 10 000 pulses and a Hanning filter in order to limit truncation noise. With 10 000 pulses, the induced linewidth is about 120 MHz, which is a numerical artifact that occurs due to the finite length of the pulse string. This linewidth is large compared to the experimentally-observed linewidths [3] that range between 1 kHz and 1 MHz. In Fig. 4.b, we show the PSD that is generated using Eq. 8. The PSD in Fig. 4.b is the same as in Fig. 4.a. We show an expanded view of the two overlap regions in both sub-figures. We see that the offset between the primary comb B_0 and both the signal B_- and the idler B_+ has the same magnitude with the opposite sign in both sub-figures.

The difference between these two combs is visible in the linewidth of the comb lines in the two sub-figures. The linewidth of the comb lines in Fig. 4.b is zero. In the experiments, the actual linewidth when f - $2f$ locking is not used is primarily due to a combination of thermorefractive noise and pump noise [3, 20–23]. These effects could be included in a straightforward way to the comb generated using Eq. 8. Using Eq. 6, it would be necessary to use a string that is long enough to resolve the linewidth, which in the case of a linewidth of 1 MHz would require on the order of 10^9 pulses and in the case of a linewidth of 1 kHz would require on the order of 10^{12} pulses since the numerically-induced linewidth is inversely proportional to the number of pulses. A pulse string of length 10^9 is already too long to be practical. For comparison purposes, we note that the simulation reported in Fig. 4.a took about 20 minutes of CPU time on a high-performance workstation, while the simulation reported in Fig. 4.b takes between one and two minutes.

We next turn to the soliton-OPO effect that was observed in [7]. We will assume that the energy in the primary color is large compared to the energy in the signal, which is again large compared to the energy in the idler color. For the simulations in Figs. 3 and 4, we find $U_-/U_0 = 1.6 \times 10^{-2}$ and $U_+/U_0 = 1.1 \times 10^{-5}$, where $U_0 = \int_{-\infty}^{\infty} |b_0|^2 d\phi/2\pi$, $U_- = \int_{-\infty}^{\infty} |b_-|^2 d\phi/2\pi$, and $U_+ = \int_{-\infty}^{\infty} |b_+|^2 d\phi/2\pi$; so, this assumption is well-justified. In our simulations, the energy of the pump color was 0.43 nJ, corresponding an output power in the pump comb of 0.43 mW. Given this scaling, we can first linearize Eq. 8b, and we obtain

$$\begin{aligned} \frac{\partial b_-(\phi, t)}{\partial t} = & \left(-\frac{l}{2} + i\alpha_- \right) b_-(\phi, t) + \sum_{\mu'} [\beta\mu' + D_{\text{int}}(\mu' + \mu_-)] B_-(\mu', t) \exp(-i\mu' \phi) \\ & - 2i\gamma |b_0(\phi, t)|^2 b_-(\phi, t) + F_-, \end{aligned} \quad (9)$$

where $\alpha_- = \alpha_0 - \delta\omega + \beta\mu_-$. In the wavenumber domain, this equation becomes

$$\begin{aligned} \frac{dB_-(\mu, t)}{dt} = & \left[-\frac{l}{2} + i\alpha_- + i\beta\mu' + iD_{\text{int}}(\mu + \mu') \right] B_-(\mu, t) \\ & - 2i\gamma \sum_{\rho, \sigma} B_0(\rho) B_0^*(\sigma) B_-(\mu' + \sigma - \rho) + F_- \delta(\mu'). \end{aligned} \quad (10)$$

We next assume that $B_0(0, t)$ and $B_-(0, t)$ dominate the sum in Eq. 10. This assumption is reasonable since they are resonant with the pumps. The integrated dispersion changes rapidly in the neighborhood of μ_- ; so, it is also reasonable to expand $\alpha_- + \beta\mu' + D_{\text{int}}(\mu' + \mu_-) \simeq E_- + E'_-\mu'$, keeping only the first two terms in the difference expansion. Equation 10 now simplifies to

$$\begin{aligned} \frac{dB_-(\mu', t)}{dt} = & \left(-\frac{l}{2} + iE_- + iE'_-\mu' \right) B_-(\mu', t) - 2i\gamma [B_0^*(0, t) B_-(0, t) B_0(\mu', t) \\ & + B_0(0, t) B_-(0, t) B_0^*(-\mu', t)] + F_- \delta(\mu'). \end{aligned} \quad (11)$$

In steady state, we then find

$$B_-(\mu') = 2\gamma \left(i\frac{l}{2} + E_- + E'_-\mu' \right)^{-1} [B_0^*(0) B_-(0) B_0^*(\mu') + B_0(0) B_-(0) B_0^*(-\mu')], \quad (12)$$

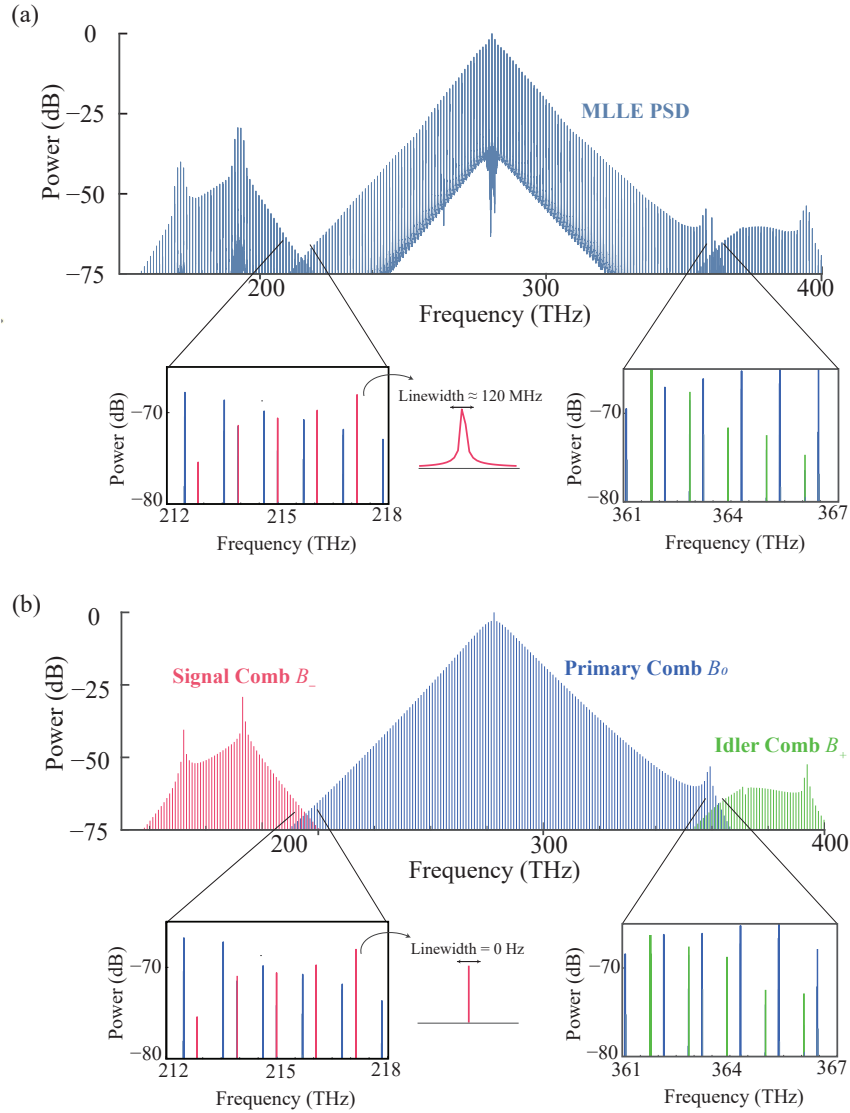


Fig. 4. The PSD of the output comb, based on (a) Eq. 6 and on (b) Eq. 8. We show the primary comb B_0 in blue, the signal comb B_- in red, and idler comb B_+ in green. The PSDs of the calculated combs are nearly identical. Additionally, we show the lower and upper frequency overlap regions for both calculated combs. The offset between the lines of the primary comb and idler comb is equal and opposite of the offset between the lines of the primary and signal comb and has a magnitude of 330 GHz. The results of both calculations are identical. The only difference is in the linewidth of the individual comb lines, which is approximately 120 MHz in (a) due to the finite number of pulses in the pulse string, but is zero in (b).

which is resonant when $\mu' \simeq -E_-/E'_-$, as observed in [7]. The mode number spectrum of B_0 is imprinted on B_- with an offset that is determined by β and D_{int} in the neighborhood of $\mu = \mu_-$.

We determine the spectrum of $B_+(\mu'', t)$ in an analogous fashion. The spectrum of B_+ is entirely driven by B_0 and B_- . We define E_+ and E'_+ as the first two terms in the difference expansion of $\alpha + \delta\omega_-$. We then find in steady state

$$B_+(\mu'') = 2\gamma \left(i\frac{l}{2} + E_+ + E'_+\mu'' \right)^{-1} B_0(0)B_-^*(0)B_0(\mu''), \quad (13)$$

and find that the spectrum of B_0 is imprinted on B_+ with a resonance at $\mu'' \simeq -E_+/E'_+$.

In Fig. 5, we compare the mode number spectra that are computed using Eqs. 8b and 8c to the spectra that are computed using Eqs. 12 and 13. We see that the results are nearly the same. In Fig. 5.c, we show $\text{Re}(b_-)$ and $\text{Re}(b_+)$. The tanh-like shape of $\text{Re}(b_-)$ is apparent and will be the subject of a future publication. This result both explains the soliton-OPO effect that was observed in [7] and indicates the conditions that are required to observe it.

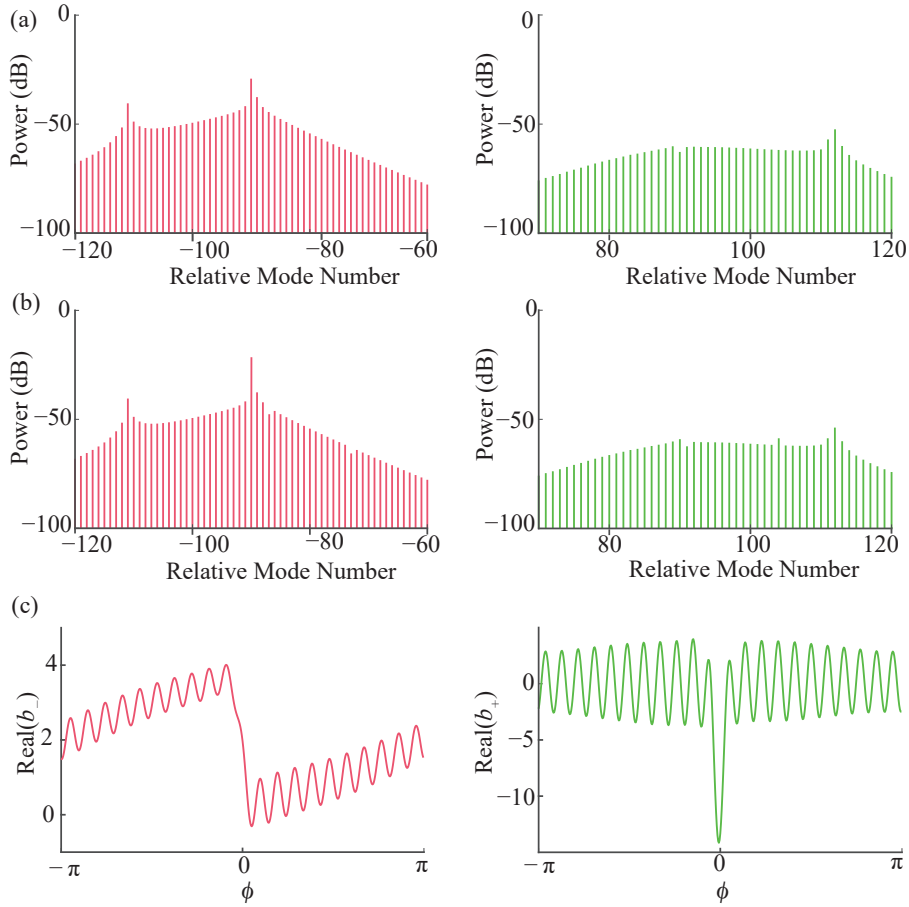


Fig. 5. We compare $|B_-(\mu')|^2$ and $|B_+(\mu'')|^2$ computed using (a) Eqs. 8b and 8c and using (b) Eqs. 12 and 13. In (c), we show $\text{Re}(b_-)$ and $\text{Re}(b_+)$. The tanh-like shape of $\text{Re}(b_-)$ is apparent.

4. Conclusions

In this paper, we derive three-wave equations that govern the waveform evolution in a microresonator that is pumped at two frequencies in a regime in which a multi-color soliton is produced in the microresonator cavity. Multi-color solitons are waveforms that have a single group velocity and hence a single f_{rep} while having two or more phase velocities and hence two different carrier envelope offsets f_{ceo} . They appear in microresonators whose integrated dispersion D_{int} , evaluated at the frequency of the primary pump, is nearly quartic with zero crossings that are far removed from the primary pump. Unless the secondary pump's frequency is tuned close to a comb line of the primary comb, multi-color solitons form. Multi-color solitons play a critical role in the synchronization process.

We began with a derivation of the three-wave equations, and we demonstrated that these equations reproduce the multi-color soliton solutions that are obtained from a modified LLE that uses a realistic dispersion profile. A periodic stream of multi-color solitons produces an interleaved frequency comb when the stream is detected and its frequency spectrum analyzed outside the microresonator. Because there are two or more carrier envelope offsets, the relative phase of the colors slip by a constant phase on every round trip. We showed that the modified LLE can reproduce the observations if one generates a long string of pulses and calculates the Fourier transform of the string. We then showed that we can use the three-wave equations to shortcut this detection process.

Finally, we used the three-wave equations to explain the soliton-OPO effect that was observed experimentally [7] and to determine the conditions under which it is expected to appear. In this microresonator, the zero-crossings of D_{int} are too far from the primary pump resonance to generate a doubly-dispersive wave. However, we show that the primary comb mode number spectrum B_0 imprints itself on both the signal comb mode number spectrum B_- and the spectrum of the idler comb B_+ that is generated by the soliton-OPO process. As a result the total bandwidth of the entire frequency comb can be greatly extended.

There is much that can be done with these equations to study waveforms in microresonator systems. As one example, they can be used to determine the stability of the multi-color solitons and their response to noise. These equations can also be used as a starting point for a careful asymptotic analysis of multi-color solitons. Moreover, the soliton-OPO effect is in many ways analogous to the CW-OPO effect, and it can be cascaded, opening up a path to creating a frequency comb spectrum in otherwise difficult-to-access frequency regimes. These equations are a useful starting point for analyzing soliton-OPO cascades. We have barely scratched the surface of what can be learned from these equations.

5. Acknowledgements

We thank M. Erkintalo and A. Matsko for pointing us to work that is similar in some respects to the multi-color solitons that we describe here.

6. Funding

Work at UMBC was supported by NSF grant ECCS-1807272, by AFOSR grant FA9550-20-1-0357, and by a collaborative agreement 2022138-142232 with the National Center for Manufacturing Sciences as a sub-award from US DoD cooperative agreement HQ0034-20-2-0007. Work at the Joint Quantum Institute/NIST was supported by the Space and Vehicles Directorate of the Air Force Research Laboratory and the NIST-on-a-chip program of the National Institute of Standards and Technology.

7. Disclosure

The authors declare no conflicts of interest.

8. Data Availability Statement

Data underlying the results presented in this paper are available upon reasonable request.

References

1. G. Moille, J. Stone, M. Chojnacky, *et al.*, “Kerr-induced synchronization of a cavity soliton to an optical reference,” *Nature* **624**, 267–274 (2023).
2. M. Tan and D. Moss, “The trick that could put an optical clock on a chip,” *Nature* **624**, 256–257 (2023).
3. G. Moille, P. Shandilya, J. Stone, *et al.*, “All-optical noise quenching of an integrated frequency comb,” arXiv:2405.01238 (2 May 2024).
4. S. Zhang, J. M. Silver, L. D. Bino, *et al.*, “Sub-milliwatt-level microresonator solitons with extended access range using an auxiliary laser,” *Optica* **6**, 206–212 (2019).
5. Z. Lu, W. Wang, W. Zhang, *et al.*, “Deterministic generation and switching of dissipative Kerr soliton in a thermally controlled micro-resonator,” *AIP Adv.* **9**, 025314 (2019).
6. H. Zhou, Y. Geng, W. Cui, *et al.*, “Soliton bursts and deterministic dissipative Kerr soliton generation in auxiliary-assisted microcavities,” *Light. Sci. & Appl.* **8**, 50 (2019).
7. G. Moille, E. F. Perez, J. R. Stone, *et al.*, “Ultra-broadband Kerr microcomb through soliton spectral translation,” *Nat. Commun.* **12**, 7275 (2021).
8. S. Trillo, S. Wabnitz, E. M. Wright, and G. I. Stegeman, “Optical solitary waves induced by cross-phase modulation,” *Opt. Lett.* **13**, 871–873 (1988).
9. Q.-F. Yang, X. Yi, K. Y. Yang, and K. Vahala, “Stokes solitons in optical microcavities,” *Nat. Phys.* **13**, 53–57 (2016).
10. C. R. Menyuk, “Stability of solitons in birefringent optical fibers. I: Equal propagation amplitudes,” *Opt. Lett.* **12**, 614–616 (1987).
11. M. Jankowski, A. Marandi, C. R. Phillips, *et al.*, “Temporal solitons in optical parametric oscillators,” *Phys. Rev. Lett.* **120**, 053904 (2018).
12. Y. Ding, Z. Wei, Y. Wang, *et al.*, “Theoretical analysis of microcavity solitons reinforced by $\chi^{(2)}$ and $\chi^{(3)}$ nonlinearities,” *Phys. Rev. Lett.* **132**, 013801 (2024).
13. R. Luo, H. Liang, and Q. Lin, “Multicolor cavity soliton,” *Opt. Express* **24**, 16777–16787 (2016).
14. C. Silvestri, J. Widjaja, A. Lin, *et al.*, “Theory of multicolor soliton microcombs,” *Opt. Lett.* **50**, 2073–2076 (2025).
15. A. B. Matsko, A. A. Savchenko, W. Liang, *et al.*, “Mode-locked frequency combs,” *Opt. Lett.* **36**, 2845–2847 (2011).
16. S. Coen, H. G. Randle, T. Sylvestre, and M. Erkintalo, “Modeling of octave-spanning Kerr frequency combs using a generalized mean-field Lugiato–Lefever model,” *Opt. Lett.* **38**, 37–39 (2013).
17. Y. K. Chembo and C. R. Menyuk, “Spatiotemporal Lugiato–Lefever formalism for Kerr-comb generation in whispering-gallery-mode resonators,” *Phys. Rev. A* **87**, 053852 (2013).
18. Q. Li, T. C. Briles, D. A. Westly, *et al.*, “Stably accessing octave-spanning microresonator frequency combs in the soliton regime,” *Optica* **4**, 193–203 (2017).
19. G. Moille, C. Li, J. Stone, *et al.*, “Two-dimensional nonlinear mixing between a dissipative Kerr soliton and continuous waves for a higher-dimension frequency comb,” arXiv:2303.10026v2 (20 Mar 2023).
20. J. Lim, A. A. Savchenko, E. Dale, *et al.*, “Chasing the thermodynamical noise limit in whispering-gallery-mode resonators for ultrastable laser frequency stabilization,” *Nat. Commun.* **8**, 8 (2017).
21. J. R. Stone, T. C. Briles, T. E. Drake, *et al.*, “Thermal and nonlinear dissipative-soliton dynamics in Kerr-microresonator frequency combs,” *Phys. Rev. Lett.* **12**, 063902 (2018).
22. J. Lim, W. Liang, A. A. Savchenko, *et al.*, “Probing 10 μ K stability and residual drifts in the cross-polarized dual-mode stabilization of single-crystal ultrahigh-Q optical resonators,” *Light. Sci. Appl.* **8**, 1 (2019).
23. F. Lei, Z. Ye, O. B. Helgason, *et al.*, “Optical linewidth of soliton microcombs,” *Nat. Commun.* **13**, 3161 (2022).